Magma chamber growth during inter-caldera periods: insights from thermo-mechanical modeling with applications to Laguna del Maule, Campi Flegrei, Santorini, and Aso

Meredith Townsend [a,b] *, Christian Huber [a], Wim Degruyter [c], Olivier Bachmann [d]

[a] Department of Earth, Environmental, and Planetary Sciences, Brown University, 324 Brook Street, Providence, RI 02906, USA

[b] Department of Earth Sciences, University of Oregon, 100 Cascade Hall, Eugene, OR 97403, USA

[c] School of Earth and Ocean Sciences, Cardiff University, Main Building, Park Place, Cardiff, CF10 3AT, United Kingdom

[d] Department of Earth Sciences, ETH Zurich, Sonneggstrasse 5, 8092 Zurich, Switzerland

Keywords: Magma chambers, caldera cycles, eruption frequency, eruption volume, magmatic volatiles

Key points:

- Coupled thermo-mechanical modeling suggests that magma chambers grow when recharge and viscous relaxation of the crust are fast compared to chamber cooling
- Magma chambers containing exsolved volatiles may shrink over time despite constant recharge because high magma compressibility leads to large eruption volumes
- Eruptive phases at Laguna del Maule, Campi Flegrei, Santorini and Aso reflect growth of chambers; amount of growth can be estimated from eruption frequency and size

* Corresponding author: Tel.: +1 434 390-7952

E-mail addresses: meredith_townsend@brown.edu (M.R. Townsend), christian_huber@brown.edu (C. Huber), degruyterw@cardiff.ac.uk (W. Degruyter), olivier.bachmann@erdw.ethz.ch (O. Bachmann)

Abstract

Crustal magma chambers can grow to be hundreds to thousands of cubic kilometers, potentially feeding catastrophic caldera-forming eruptions. Smaller-volume chambers are expected to erupt frequently and freeze quickly; a major outstanding question is how magma chambers ever grow to the sizes required to sustain the largest eruptions on Earth. We use a thermo-mechanical model to investigate the primary factors that govern the extrusive:intrusive ratio in a chamber, and how this relates to eruption frequency, eruption size, and long-term chamber growth. The model consists of three fundamental timescales: the magma injection timescale τ_{in}, the cooling timescale τ_{cool}, and the timescale for viscous relaxation of the crust τ_{relax}. We estimate these timescales using geologic and geophysical data from four volcanoes (Laguna del Maule, Campi Flegrei, Santorini, Aso) to compare them with the model. In each of these systems, τ_{in} is much shorter than τ_{cool} and slightly shorter than τ_{relax}, conditions that in the model are associated with efficient chamber growth and simultaneous eruption. In addition, the model suggests that the magma chambers underlying these volcanoes are growing at rates between ~10^{-4} - 10^{-2} km^3/yr, speeding up over time as the chamber volume increases. We find scaling relationships for eruption frequency and size that suggest that as chambers grow and volatiles exsolve, eruption frequency decreases but eruption size increases. These scaling relationships provide a good match to the eruptive history from the natural systems, suggesting the relationships can be used to constrain chamber growth rates and volatile saturation state from the eruptive history alone.

Plain Language Summary

Magma chambers in the earth's crust grow by incremental addition of new magma from deeper reservoirs, and over time can reach volumes that would fill the entire Grand Canyon. However, small magma chambers in the earliest stages of formation are prone to frequent eruptions and will lose heat quickly to the surrounding crust, both of which supposedly impede growth. Therefore, an important question is how magma chambers can possibly grow to such large sizes. Here, we present results of physics-based modeling aimed at understanding what conditions allow magma chambers to grow. We test effects of chamber size, rate of magma supply, water content in the magma, and plasticity of the crust hosting the chamber. Results suggest that growth is promoted when chambers cool slowly and are hosted within pliable crust that can easily relax pressures that build within the chamber. Surprisingly, we found that for a particular range of crustal pliability, growth is accompanied by frequent volcanic eruptions. We compared these results to four large volcanoes in Chile, Italy, Greece, and Japan. Model predictions for eruption frequency and chamber growth rates are a good match to what we observe at these volcanoes from the rock record and active monitoring systems.

1. Introduction

The growth of crustal magma chambers largely governs the frequency and size of volcanic eruptions and plays a critical role in the thermal and chemical evolution of the planet. Field studies of plutons (C. F. Miller et al., 2011; R. B. Miller & Paterson, 2001; Paterson & Miller, 1998; Wiebe, 1994; Wiebe & Collins, 1998) and eruptive deposits (Chamberlain, Wilson, Wooden, Charlier, & Ireland, 2014; Charlier, Wilson, & Davidson, 2008; Matthews, Vazquez, & Calvert, 2015), analogue experiments (Snyder & Tait, 1995), and numerical models (Annen, 2009; Jellinek & DePaolo, 2003; Karlstrom, Dufek, & Manga, 2009) have illuminated the physical processes by which magma chambers are assembled, typically by the episodic injection of magma via dikes ascending from deeper reservoirs. However, we do not yet understand what determines the proportion of magma that ultimately remains in the crust relative to the amount erupted (Black & Manga, 2016; White, Crisp, & Spera, 2006) and how this relates to the long-term growth of eruptible portions of the reservoir, referred to here as magma chambers. Thermal and mechanical models (Annen, 2009; Degruyter & Huber, 2014; Jellinek & DePaolo, 2003) suggest that for a given rate of magma supply, smaller chambers are more likely to erupt and freeze, while larger chambers favor magma storage, which begs the question: How do magma chambers grow to the volumes required to sustain the largest eruptions on Earth?

Large silicic volcanoes are capable of erupting hundreds to thousands of cubic kilometers of material, typically accompanied by catastrophic collapse of the magma chamber roof to form a caldera (de Silva & Gregg, 2014; W. Hildreth, 1981; Lipman, Steven, & Mehnert, 1970; Sparks et al., 1985). These caldera-forming events can occur multiple times at the same volcano but typically happen infrequently, separated by tens to hundreds of thousands of years (Bevilacqua et al., 2018; Christiansen, 2001; Druitt & Francaviglia, 1992; Kaneko, Kamata, Koyaguchi, Yoshikawa, & Furukawa, 2007; Orsi, DeVita, & diVito, 1996; Wilson et al., 1995). Following large caldera-forming events, eruptions tend to be smaller-volume and higher-frequency, indicating a significant reduction in chamber size (Degruyter, Huber, Bachmann, Cooper, & Kent, 2016; Forni, Degruyter, Bachmann, De Astis, & Mollo, 2018; Parks et al., 2012; Singer et al., 2014). In this study, we focus on how small-volume post-caldera magma chambers grow to the sizes that host catastrophic caldera-forming eruptions, with a particular interest in the following questions: What controls the growth rates of magma chambers and the

time between catastrophic caldera-forming events? How does growth of the magma chamber relate to the frequency and size distribution of eruptions that occur during the inter-caldera period, and is there any way to use these eruptive characteristics to infer where a volcano is in its caldera cycle?

Growth of crustal chambers undeniably requires a sustained supply of magma; however, we posit that the partitioning of ascending magma between the surface and crust (the ratio of mass erupted to added, M_{er}:M_{add}) is also governed by the mechanics of the magma chamber. Degruyter and Huber (2014) constructed a thermo-mechanical framework to study the frequency of eruptions originating from shallow chambers fed by a supply of magma. The framework compares timescales for magma injection, cooling, and viscous relaxation of the surrounding crust:

$$\tau_{in} = \frac{\rho V}{\dot{M}_{in}} \quad (1)$$

$$\tau_{cool} = \frac{R^2}{\kappa} \quad (2)$$

$$\tau_{relax} = \frac{\eta_r}{\Delta P_c} \quad (3)$$

where the governing parameters include the chamber volume $V = \frac{4}{3}\pi R^3$, bulk magma density ρ, mass recharge rate $\dot{M}_{in}$, thermal diffusivity κ, host-rock viscosity η_r, and the critical overpressure in the chamber required to initiate an eruption ΔP_c (Rubin, 1995). Eruptions are typically envisaged as the result of magma recharge that is large enough and rapid enough to both pressurize the chamber and prevent solidification (Annen, 2009; Gelman, Gutierrez, & Bachmann, 2013; Jellinek & DePaolo, 2003). In other words, an eruption may be triggered if $\tau_{in} < \tau_{relax}$ and $\tau_{in} < \tau_{cool}$. However, eruptions also may be triggered by the exsolution of magmatic volatiles during crystallization and second boiling, (Black & Manga, 2017; Blake, 1984; Forni et al., 2018; M. J. Stock, Humphreys, Smith, Isaia, & Pyle, 2016; Tait, Jaupart, &

Vergniolle, 1989), which generally would occur when $\tau_{cool} < \tau_{in}$ and $\tau_{cool} < \tau_{relax}$. We can visualize the eruption mechanisms and eruption frequency as a function of the fundamental timescales using a regime diagram from Deguyter and Huber (2014) shown in Figure 1. In the diagram, $\theta_1 = \frac{\tau_{cool}}{\tau_{in}}$ and $\theta_2 = \frac{\tau_{relax}}{\tau_{in}}$. Eruptions triggered by second boiling occur when cooling is the fastest process and the crust behaves elastically (Region 1, $\theta_1 < 1$ and $\theta_2 > \theta_1$). Eruptions triggered by mass injection occur when injection is faster than cooling and the crust behaves elastically (Region 2, $\theta_1 > 1$ and $\theta_2 > 1$). Finally, no eruptions are predicted to occur if crustal relaxation is faster than both cooling and injection (Region 3).

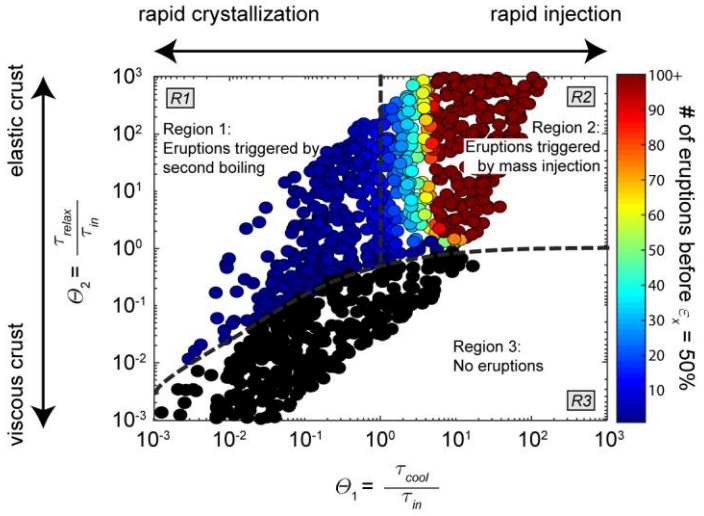

Figure 1. Regime diagram modified from Degruyter and Huber (2014) showing the relationship between eruption frequency and triggering mechanism, and the timescales for magma recharge, chamber cooling, and viscous relaxation of the host rock. Circles are colored by the number of eruptions that occur before the chamber freezes (before crystallinity reaches 50%), here plotted for a parent magma with 5 wt% H_2O initially at 200 MPa and critical overpressures of 20 MPa.

This idealized model can explain, to a first order, trends in eruption frequency and volume for a number of long-lived volcanic systems (Degruyter et al., 2016; Degruyter, Huber, Bachmann, Cooper, & Kent, 2017; Forni et al., 2018). We first extend the model to account for the transition of magma between volatile undersaturation and volatile saturation/exsolution to form a magmatic volatile phase (MVP). We then use this framework to consider how the cooling, injection, and viscous relaxation timescales (τ_{cool}, τ_{in}, and τ_{relax}) influence the growth of the chamber and the proportion of magma that is erupted versus stored (M_{er}:M_{add}). The high compressibility of the MVP is expected to decrease the eruption frequency but increase the eruption size from shallow magma chambers (Bower & Woods, 1997; Caricchi, Annen, Blundy, Simpson, & Pinel, 2014; Degruyter et al., 2016; Huppert & Woods, 2002; Woods & Huppert,

2003); we explore how this competition ultimately impacts the long-term growth and stability of the chamber.

The key timescales (τ_{cool}, τ_{in}, and τ_{relax}) and the magmatic volatile content can be variably constrained at caldera systems by a combination of geologic, petrologic, and geophysical data. In this paper, we begin by summarizing constraints on τ_{cool}, τ_{in}, and τ_{relax} from inter-caldera eruptive episodes four silicic systems (Laguna del Maule, Campi Flegrei, Santorini, and Aso), which we use to compare with the results of the thermo-mechanical model for magma chamber growth. Based on these comparisons, we seek scaling relationships that can be used to infer chamber growth and volatile exsolution from the eruptive history alone (frequency and size distribution).

2. Evolution of magma chambers in caldera systems

Constraining the timescale for magma injection, $\tau_{in} = \frac{\rho V}{\dot{M}_{in}}$, requires an estimate for the rate of magma supply $\dot{M}_{in}$ to the chamber. In reality, magma likely is delivered in pulses as dikes propagate into and feed the chamber. At active volcanoes, these events manifest as (1) episodes of surface uplift as the underlying chamber inflates (Le Mevel, Gregg, & Feigl, 2016; Parks et al., 2012), and (2) episodes of increased seismicity (McKee et al., 1984; Papadopoulos, Sachpazi, Panopoulou, & Stavrakakis, 1998). The magnitude and distribution of vertical and horizontal surface displacements are related to the depth, shape, and volume change of the chamber, which are used to estimate the volumetric magma inflow rate. These rates typically are significantly greater (order ~0.01 km^3/yr) than long-term average magma supply rates (order ~0.001 km^3/yr), which are determined by other means; for example, the average rate of volcanic output can be used to place a minimum bound on the long-term supply rates, and in some cases structural and geomorphic data permit estimates of the volume added to the crust over geologic periods of time (Singer et al., 2018). Thermally and mechanically, we expect little difference in the average behavior (e.g. eruption frequency) of magma chambers subject to high-rate, short duration or low-rate, long-duration recharges for a similar long-term average inflow rate (Degruyter et al., 2016). We therefore estimate long-term averaged values and use a constant mass inflow rate in the model.

Geophysical data from seismic, gravity, and magnetotelluric surveys can provide constraints on the present-day volume V of crustal chambers at active volcanoes (Magee et al., 2018), which are required to estimate both τ_{in} and $\tau_{cool} = \frac{R^2}{\kappa}$. Petrologic data from eruptive deposits constrain magma storage conditions such as pressure, temperature, and dissolved volatile content, from which we can infer the presence of a magmatic volatile phase (MVP) within chambers prior to eruptions.

An estimate of the crustal relaxation timescale $\tau_{relax} = \frac{\eta_r}{\Delta P_c}$ requires constraints on the effective viscosity η_r of the host-rock surrounding the chamber, and the critical overpressure ΔP_c required to initiate an eruption. Jellinek and DePaolo (2003) estimate ΔP_c required to propagate a rhyolite dike to the surface and find that ΔP_c ~10 – 40 MPa, based on scaling of the cooling rate of the dike. Here we adopt a value of 20 MPa. Although host-rock viscosity can vary by a few orders of magnitude depending on the lithology, temperature, and state of stress, we use a single value for effective viscosity of 10^{19} Pa· s for each of the magmatic systems presented here, resulting in τ_{relax} ~16 ky. This value would be consistent with a chamber at ~7.5 km depth for a normal geothermal gradient (30 °C/km), or shallower depths with more thermally mature crust (Karlstrom, Dufek, & Manga, 2010). For the shallower volcanic systems presented here, greater values of viscosity may be more appropriate. We note that since $\tau_{relax} \propto \eta_r$ the effects of greater viscosity may be seen by shifting τ_{relax} and $\theta_2 = \frac{\tau_{relax}}{\tau_{in}}$ proportionally.

2.1 Laguna del Maule, Chile

Laguna del Maule Volcanic Field is located ~80 km east of the active volcanic arc in the southern Andes and currently is one of the best studied caldera systems in the world (http://geoscience.wisc.edu/rhyolitic/). The system comprises ~350 km^3 of lavas and tuffs of basaltic to rhyolitic composition erupted throughout the Pleistocene (Wes Hildreth, Godoy, Fierstein, & Singer, 2010). Evidence of at least two catastrophic caldera-forming eruptions include a dacite ignimbrite aged ~1.5 Ma and a ~80 km^3 biotite-rhyodacite tuff aged ~950 ka (Wes Hildreth et al., 2010; Singer et al., 2014). The last major large-volume eruption produced ~20 km^3 of rhyolitic tephra and coincides with deglaciation at ~25 ka (Singer et al., 2014). Since this time, over 13 km^3 of crystal-poor rhyolite (<10% phenocrysts) have erupted, and the

volcanic activity was concentrated into two phases: an early post-glacial period from ~25-19 ka that output ~1.5 km^3 from about 20 eruptions, and a Holocene phase from ~8 – 1.9 ka that output >3.3 km^3 from only about 10 eruptions (Singer et al., 2014)(Table 1). Magma storage conditions during these phases were relatively cold and wet; water contents dissolved in the melt range from about 4.4 – 6.0 wt% for both rhyolites and rhyodacites (Andersen et al., 2018). Magnetite-ilmenite thermometry from samples of both early post-glacial and Holocene eruptions suggests temperatures of ~760 – 850 °C, and amphibole thermobarometry indicates pressures of ~180 – 250 MPa (Andersen et al., 2017). At these pressures, temperatures, and water contents, rhyolitic magma likely is water-saturated.

Since 2007, a 200 km^2 area of the Laguna del Maule lake basin has been uplifting at a rate of about ~25 cm/yr, inferred to be due to intrusion of magma to a sill-shaped body at ~5 km depth at a rate of ~0.025 – 0.05 km^3/yr (Feigl et al., 2014; Le Mevel et al., 2016). The current inflation is thought to exemplify one of several episodic magma recharge events that occurred throughout the Holocene, accumulating in over 60 meters of uplift since 9.4 ka and supplying ~13 km^3 of magma, indicating a long-term average recharge rate of 0.0023 km^3 /yr (Singer et al., 2018). A gravity anomaly ~2 – 4 km beneath the lake is interpreted as a low-density (1800 – 1900 kg/m^3), crystal-poor (< 50%), and volatile-rich zone about 30 km^3 in volume embedded within a larger (>100 km^3) zone of crystal rich (> 70%) cumulate mush (C. A. Miller, Williams-Jones, Fournier, & Witter, 2017). The ratio of magma erupted (~8.4 km^3) to the volume of magma added (~13 km^3) during the last ~9.4 ka suggests that magma injection has led to reservoir growth throughout the Holocene and possibly since the last major plinian eruption of the Rhyolite of Laguna del Maule (*rdm*) at ~25 ka. Using a chamber volume of ~ 30 km^3 from the gravity data (C. A. Miller et al., 2017), and the long-term magma supply rate (0.0023 km^3 /yr), the injection timescale τ_{in} ~13 ky and the cooling timescale τ_{cool} ~ 117 ky. Prior to the Holocene phase, when the chamber was likely smaller by >13 km^3, these timescales would have been closer to τ_{in} ~7.5 ky and τ_{cool} ~ 79 ky (Table 1).

2.2 Campi Flegrei, Italy

Campi Flegrei, located a few kilometers west of Naples and home to over 1.5 million people, consists of two nested calderas associated with the ~300 km^3 eruption of the Campanian

Ignimbrite (CI) at ~39 ka and the ~40 km^3 Neapolitan Yellow Tuff (NYT) at ~15 ka (Deino, Orsi, de Vita, & Piochi, 2004). Since the NYT, about 60 more eruptions have occurred ranging in composition from basaltic trachy-andesite to trachy-phonolite, arriving in three epochs of activity (Bevilacqua, Flandoli, Neri, Isaia, & Vitale, 2016; Di Vito et al., 1999; Orsi, Di Vito, & Isaia, 2004; Smith, Isaia, & Pearce, 2011): The first epoch was from ~15.0 – 9.5 ka and included about 34 explosive eruptions totaling ~5.4 km^3; the second epoch was the shortest, lasting from ~8.6 – 8.2 ka with 6 explosive eruptions totaling ~0.69 km^3 (Smith et al., 2011); the third epoch from ~4.8 – 3.8 ka included 16 explosive eruptions and 4 effusive eruptions totaling ~2.5 km^3 (Smith et al., 2011) (Table 1). Following the CI eruption at ~39ka, magma storage conditions were relatively hot (1000-1090 °C), dry (3-5 wt% water), and mafic, evolving to colder (880-930 °C) and wetter conditions (5-7 wt% water) just prior to the eruption of the NYT (Forni et al., 2018). After the NYT, the reservoir become once again hot, dry, and mafic (1070-1130 °C with 0.2 – 3.5 wt% water), progressing to colder and wetter conditions throughout the 1^{st}, 2^{nd}, and 3^{rd} epochs (900-1080 °C and 3-6 wt%) (Forni et al., 2018; M. Stock et al., 2018). The most recent eruption of Monte Nuovo in 1538 continued on this trend (870-920 °C and 5-7 wt%) (Forni et al., 2018).

The minimum magma supply rates for the three epochs constrained from eruptive volumes are ~0.001 km^3/yr, ~0.0017 km^3/yr, and ~0.0025 km^3/yr, respectively. A maximum bound on magma supply rate is found by considering an individual recharge event; for example, using the estimate of Di Vito et al. (2016) for a volume change of ~0.93 to 0.95 km^3 over the period 1400-1536 AD gives a magma recharge rate of ~0.007 km^3/yr. To estimate the injection timescale for the Campi Flegrei magma chamber, we use an intermediate estimate for the long-term magma supply rate of ~0.003 km^3/yr. Geophysical surveys indicate the presence of a shallow magmatic body, although the volume and distribution of melt is not well constrained (Calo & Tramelli, 2018; Fedi et al., 2018; Zollo et al., 2008). Recent modeling by Forni et al. (2018) find a good match between the predicted and estimated cumulative eruptive volumes for each of the three epochs by using an initial magma chamber volume of ~2.5 km^3 that grows to ~11 km^3 by the end of the third epoch. Using these estimates for chamber volume and magma supply rates, we estimate that τ_{in} would have increased from ~0.8 ky during the first epoch to ~3.5 ky during the third epoch. τ_{cool} would have increased from ~22.5 to ~60 ky (Table 1).

2.3 Santorini, Greece

Santorini (Thera) is a large volcanic complex within the Hellenic subduction zone, where explosive volcanic activity began at least ~360 ka (Druitt, Mellors, Pyle, & Sparks, 1989). Multiple, nested calderas and well-exposed volcanic stratigraphy indicate that the volcano cycles between large, explosive Plinian-style eruptions and smaller, effusive shield-building eruptions (Druitt & Francaviglia, 1992). The oldest caldera dates back to ~180 ka, followed by the Skaros caldera at ~70 ka, the Cape Riva caldera et ~21 ka, and the caldera associated with the Late-Bronze-Age (Minoan) eruption ~3600 years ago that ejected ~40 – 80 km^3 DRE and devastated Minoan settlements on the island (Druitt & Francaviglia, 1992; Johnston, Sparks, Phillips, & Carey, 2014; Sigurdsson et al., 2011). Since the Minoan eruption, at least 11 eruptions have occurred, giving an average eruption frequency of ~3 ky^{-1} (Pyle & Elliott, 2006). These eruptions have been dominantly effusive lavas that built up the Kameni islands in the center of the caldera bay, and have ranged in volume from ~0.0006 – 0.14 km^3, with the volume varying in proportion with the repose time (Parks et al., 2012). Deposits from the four major caldera-forming eruptions indicate relatively cold and wet conditions (850 – 900 °C and 2 – 7 wt% H_2O) compared to the post-caldera lavas (960 – 1012 °C and 1-4 wt% H_2O) (Barton & Huijsmans, 1986; Cadoux, Scaillet, Druitt, & Deloule, 2014; Cottrell, Gardner, & Rutherford, 1999; Druitt et al., 2016). Petrologic data combined with modeling by Degruyter et al. (2016) suggest that the magma chamber was water saturated prior to the Minoan eruption, but has been drier and possibly even undersaturated ever since.

The volume of the Minoan eruption ~3600 ka indicates that the chamber grew to volumes of ~40 – 80 km^3 over ~18 ky since the previous caldera-forming eruption, implying a long-term average magma supply rate of ~0.002 – 0.004 km^3/yr. However, approximately 7-15% of the erupted material is thought to be magma that recharged the system ~10-100 years prior (Druitt, Costa, Deloule, Dungan, & Scaillet, 2012; Flaherty et al., 2018), which would imply a more episodic recharge at a rate of ~0.05 km^3/yr. Episodic recharge also is supported by the recent inflation and seismic unrest in 2011-2012, which suggested the arrival of ~0.01 km^3 of magma to a chamber at ~3 – 6 km depth (Parks et al., 2012), giving a recharge rate of ~0.01 km^3/yr. Throughout post-Minoan times, the background average magma recharge rate has been ~0.001 km^3/yr, estimated from the volume of the dome in the caldera bay constructed since the Minoan

eruption (~2.5 km^3) and the volume of material erupted since AD 1570 (Parks et al., 2012). The small volumes and high frequencies of post-Minoan lavas suggests that the chamber was substantially smaller than it was prior to the Minoan eruption; the model by Degruyter et al. (2016) shows a good fit to eruptive volumes using a model chamber ~10 km^3 in volume containing no exsolved volatiles. Using this volume and the estimated long-term magma supply during the post-caldera period (0.001 km^3/yr), we estimate τ_{in} ~10 ky and τ_{cool} ~57 ky. Prior to the Minoan eruption, using a chamber volume of ~50 km^3 and the long-term magma supply since the Cape Riva (~0.0028 km^3/yr), we estimate τ_{in} ~18 ky and τ_{cool} ~165 ky (Table 1).

2.4 Aso, Japan

The large volcanic complex of Aso, in Kyushu, southern Japan, has had at least four major caldera-forming eruptions: Aso-1 at 266 ka (~50 km^3), Aso-2 at 141 ka (~50 km^3), Aso-3 at 123 ka (>150 km^3), and Aso-4 at 90 ka (>600 km^3) (Kaneko et al., 2007). The extraordinary size of the two most recent caldera-forming eruptions (Aso-3 and Aso-4) suggests that the underlying magma chamber is capable of growing to several hundred cubic kilometers in volume in the span of a few tens of thousands of years. Since Aso-4 at 90 ka, eruptive activity has continued and is concentrated into two pulses: Phase 1 from ~70 – 50 ka, consisting of 18 tephra units totaling ~5 km^3, and 6 lava units totaling ~1 km^3; and Phase 2 from ~40 – 20 ka consisting of 6 tephra units totaling ~3 km^3, and 8 lava units totaling ~1.3 km^3 (Miyabuchi, 2009; Miyoshi et al., 2012). Altogether, the eruption frequency from Phase 1 (~1.2 ky^{-1}) is almost double that of Phase 2 (~0.7 ky^{-1}) while the average eruption volume is slightly greater during Phase 2 (~0.29 km^3 per eruption) compared to Phase 1 (~0.25 km^3 per eruption) (Table 1).

From the volume of post-caldera cone edifices (112 km^3) that were built over the last 90 ky, the magma supply rate at Aso is estimated to be ~0.0015 km^3/yr (Miyabuchi, 2009). A recent 3D electrical resistivity study imaged what is interpreted to be the shallow crustal reservoir, with a roof located at ~6 km depth (Hata et al., 2018), in agreement with seismic data (Sudo & Kong, 2001). The resistivity data are interpreted as showing a magma body ~6.3 km^3 in volume with melt fractions of 96-99%, contained within a mush zone ~90 km^3 with lower melt fractions (2-3%) (Hata et al., 2018). Without further constraints on historical chamber volumes over the last

90 ky, we use the present-day constraint of 6.3 km^3 to estimate τ_{in} ~4.1 ky and τ_{cool} ~41 ky (Table 1).

Volcano, epoch	Eruption frequency (ky^{-1})	Average eruption volume (km^3)	Caldera cycle (ky)	Chamber volume (km^3)	Magma supply (km^3/yr)	τ_{in} (ky)	τ_{cool} (ky)
LdM, EPG	5.5[*]	0.046[*]	550-925[§]	~17[‡#]	0.0023[†]	7.5	79
LdM, Holocene	1[*]	0.55[*]	550-925[§]	~30[^]	0.0023[†]	13	117
CF Epoch 1	6.2[†]	0.16[†]	~24[†]	~2.5[•]	0.003[†]	0.8	22.5
CF Epoch 2	15[†]	0.11[†]	~24[†]	~7[•]	0.003[†]	2.3	44
CF Epoch 3	16[†]	0.16[†]	~24[†]	~11[•]	0.003[†]	3.5	60
Santorini, post-Minoan	3[–]	0.064[–]	18 to 110[–]	~10[’]	0.001[–]	10	57
Santorini, pre-Minoan	--	--	18 to 110[–]	~50[&]	0.0028[&]	18	165
Aso Phase 1	1.2[‡]	0.25[‡]	18 to 125[+]	~6.3[!]	0.0015	4.1	41
Aso Phase 2	0.7[‡]	0.29[‡]	18 to 125[+]	~6.3[!]	0.0015	4.1	41

Table 1. Summary of constraints on eruption frequency, volume, caldera cycle length, and the timescales for injection and cooling during various eruptive phases at four different large silicic systems. LdM = Laguna del Maule; EPG = Early Post-Glacial period; CF = Campi Flegrei [*](Singer et al., 2014) [#](Singer et al., 2018) [^](C. A. Miller et al., 2017) [§](Wes Hildreth et al., 2010) [†](Smith et al., 2011) [•](Forni et al., 2018) [–](Parks et al., 2012) [&](Johnston et al., 2014) [’](Degruyter et al., 2016) [‡](Miyabuchi, 2009) [+](Kaneko et al., 2007) [!](Hata, Takakura, Matsushima, Hashimoto, & Utsugi, 2016)

3. Modeling eruption frequency, volume, and chamber growth

In this section, we present modeling results for eruption frequency and chamber growth as a function of the fundamental timescales τ_{in}, τ_{cool}, and τ_{relax}, as well as the initial water content of the magma X_{H2O}. In this way, we can compare the eruptive history at Laguna del Maule, Campi Flegrei, Santorini, and Aso to the output of the model in order to better understand the long-term evolution and growth rates of these silicic magma chambers. Furthermore, we aim to gain a broader understanding of the conditions that promote growth, and we test whether we can use changes in the frequency and size of volcanic eruptions to determine changes in the size and volatile saturation state of the underlying chamber.

3.1 Model setup and model parameters

The magma chamber model of Degruyter and Huber (2014) approximates the chamber as a sphere of radius R and volume V containing a mixture of silicate melt, solid crystals, and a magmatic volatile phase (MVP), here assumed to be water. We assume the chamber is spatially homogeneous and calculate average values of pressure, temperature, density, and crystal and MVP volume fractions. Magma recharge is a constant mass inflow rate $\dot{M}_{in}$ at a specified temperature and initial dissolved water content X_{H2O}. Recharge adds mass and energy to the chamber, while the chamber simultaneously loses heat to the surroundings. We envision the surrounding crust as a transition from a crystal-rich mush near the chamber (>50% crystals) to fully-solid crust farther away; therefore, we model the rheology as viscoelastic similar to other treatments (Del Negro, Currenti, & Scandura, 2009; Dragoni & Magnanensi, 1989; Newman, Dixon, & Gourmelen, 2006; Segall, 2016) but calculate an effective viscosity η_r from a viscosity gradient that depends on the temperature profile of the crust around the chamber. Conservation of mass, water, and energy are combined with closure equations for crystallinity, water solubility, and gas density. The melting curve implemented here uses a parameterization by (Huber, Bachmann, & Manga, 2009) for a dacite composition, and the solubility law comes from the parameterization of Dufek and Bergantz (2005) based on Zhang (1999) for solubility of water in rhyolite.

When the pressure reaches a specified critical value $P_{\text{lit}} + \Delta P_c$, an "eruption" occurs and mass is extracted from the chamber at a constant rate $\dot{M}_{out}$ (here fixed to 10^5 kg/s) until the pressure returns to the lithostatic value, here set to P_{lit} = 200 MPa. The model simulation ends when the crystal volume fraction reaches 50%, at which point we assume the magma is immobile and unlikely to erupt again.

The model has been extended to account for transitions between volatile saturation, accompanied by exsolution of gas, and undersaturation. We assume that water is the only volatile phase and that it is perfectly incompatible, so that as crystallization proceeds, all of the water remains in the melt and the concentration increases. The initial mass fraction of water in the melt within the chamber is set to $X_0^r = \frac{X_{H2O}}{\epsilon_{m,0}}$ where X_{H2O} is the total mass fraction of water in the parent magma and $\epsilon_{m,0}$ is the initial volume fraction of melt in the chamber. The concentration of water in the melt is tracked in time as crystallization increases the concentration, as recharge

adds melt at a specified concentration (here the same as the parent melt, X_{H2O}), and as eruptions remove melt at a concentration assumed to be that of the melt in the chamber X^r. When X^r is less than the water solubility m_{eq}, only two conservation equations are solved (total mass and energy); when X^r exceeds the water solubility m_{eq}, the gas volume fraction is solved for using an additional equation governing conservation of water mass.

Table 2 provides the initial conditions and range of model parameters . We use the model results to calculate the average eruption frequency *f* as a function of the mass recharge rate, initial chamber mass and volume, mass fraction of water, and host-rock effective viscosity, as we formulate this in terms of the three fundamental timescales τ_{in}, τ_{cool}, and τ_{relax}. In addition, we calculate the total mass and volume of magma erupted, summing over all of the eruptions over the course of the simulations (i.e. until ϵ_x = 50%). We compare this to the amount of mass and volume added to the system by recharge, in order to understand how the growth of the chamber by mass and volume is influenced by the three timescales and water content. Finally, we use the model results to calculate growth rates as a function of τ_{in}, τ_{cool}, and τ_{relax}, to be compared with the growth rates and caldera cycle periods estimated for the four volcanic systems discussed in Section 2.

Parameter	**Definition**	**Range of values used**
$V_0 = \frac{4}{3}\pi R_0^3$	Initial chamber volume (km^3)	0.0005 – 500 km^3
$\dot{M}_{in}$	Mass inflow rate (kg/s)	0.1 – 500 kg/s (~10^{-6} – 6*10^{-3} km^3/yr)
X_{H2O}	Water concentration of parent magma	3 – 7 wt%
P_{lit}	Ambient pressure (lithostatic)	200 MPa
ΔP_c	Critical overpressure	20 MPa
T_0	Initial chamber temperature	1200 K
T_b	Temperature at edge of viscoelastic shell (far-field temperature)	500 K

S	Radius of viscoelastic shell	$10*R_0$
κ	Thermal diffusivity of crust	10^{-6} m^2/s
$\rho_{m,0}$	Initial density of melt	2400 kg/m^3
$\rho_{x,0}$	Initial density of crystals	2750 kg/m^3
β_m, β_x, β_r	Compressibility of melt, crystals, and host rock	10^{-10} Pa^{-1}
θ_1	$\frac{\tau_{cool}}{\tau_{in}} = \frac{3}{4\pi}\frac{\dot{M}_{in}}{\kappa\rho_0 R_0}$	10^{-3} - 10^{3}
θ_2	$\frac{\tau_{relax}}{\tau_{in}} = \frac{3}{4\pi}\frac{\dot{M}_{in}\eta_{r,0}}{\Delta P_c \rho_0 R_0^3}$	10^{-3} - 10^{3}

Table 2. Values for the model parameters used to calculate eruption frequencies, volumes, and growth rates

3.2 Modeling results

3.2.1 Eruption frequency and volume

For a given chamber volume, the average eruption frequency increases with greater magma recharge rates (Figure 2a). However, the water content of the parent magma also affects eruption frequency. In the example shown in Figure 2a, the eruption frequency is plotted against magma recharge rate for a chamber with an initial volume of 5 km^3 and three different initial water contents: a dry case (3 wt%) an intermediate case (5 wt%), and a wet case (7 wt%). For the dry case, none of the simulations reach volatile saturation to form a magmatic volatile phase (MVP); in contrast, the wet case always reaches saturation and exsolves volatiles. While all of the simulations show increasing eruption frequency with magma recharge rate, the simulations with 3 wt% water resulted in frequencies that were greater by a factor of ~5-6 compared to the models with 7 wt% water. For the intermediate case, at magma recharge rates less than about 0.5 x 10^{-3} km^3/yr, eruption frequencies are similar to those for the wet case. However, once magma recharge increases to about 10^{-3} km^3/yr, the eruption frequency increases abruptly such that by M_{in} ~ 1.3 x 10^{-3} km^3/yr the intermediate case behaves identically to the dry case.

This behavior is linked to the evolution of the MVP volume fraction ϵ_g and its effect on the bulk magma compressibility β:

$$\beta = \frac{1}{\rho}\left(\epsilon_m \rho_m \beta_m + \epsilon_x \rho_x \beta_x + \epsilon_g \frac{\partial \rho_g}{\partial P}\right) \quad (4)$$

For example, in the case of 3 wt% water and M_{in} ~ 0.5 x 10^{-3} km^3/yr, the magma never reaches volatile saturation ($\epsilon_g = 0$) and the mixture remains two-phase (crystals + melt) with a consistent eruption frequency of about 18 ky^{-1} throughout its lifespan. In the case with 5 wt% water, the magma is initially MVP-free but after about 1000 years becomes saturated and exsolves an MVP (Figure 2b). Exsolution of the MVP corresponds to a sharp decrease in the eruption frequency, dropping from ~18 ky^{-1} to ~4 ky^{-1} (Figure 2b). In the wet case, the magma is initially saturated and the MVP continues to exsolve throughout the simulation, and the eruption frequency is consistently about 4 ky^{-1}.

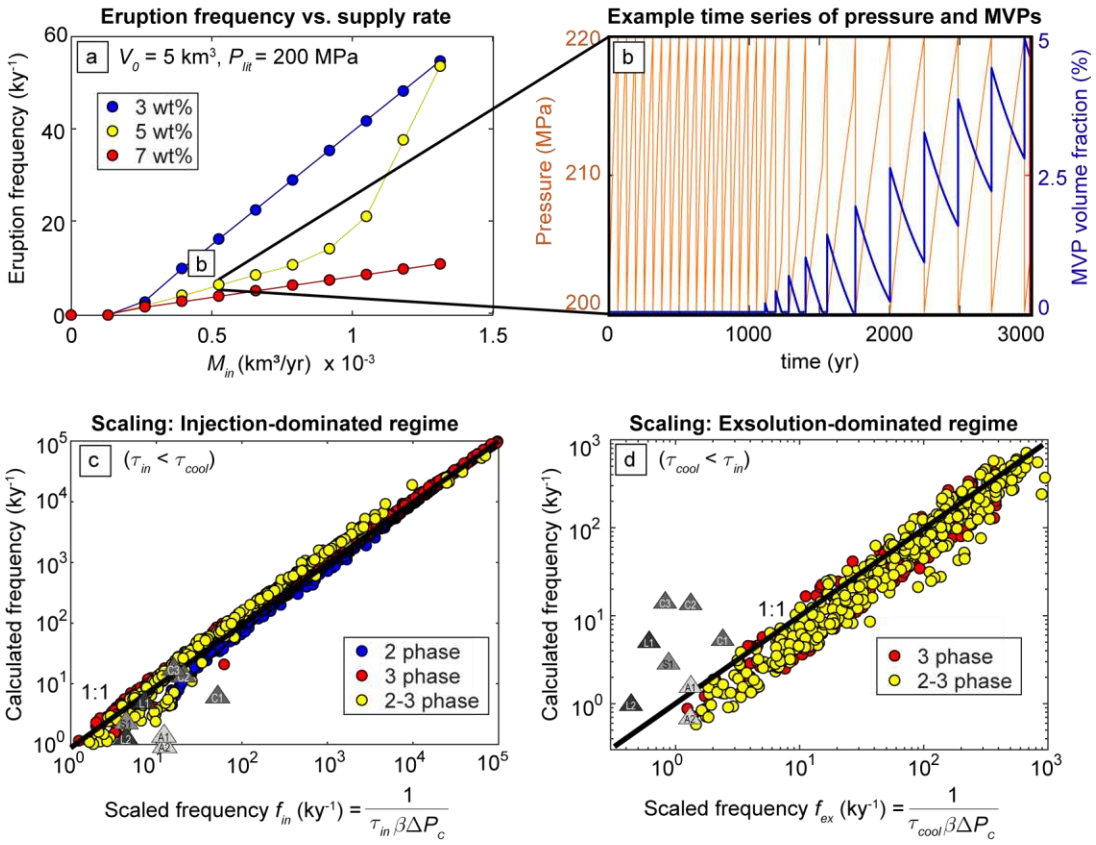

Figure 2. (a) Average eruption frequency (in ky^{-1}) as a function of magma recharge rate (km^3/yr) for three different initial water concentrations. Model labeled b is shown in detail in the right-hand panel (b) Evolution of chamber pressure and gas volume fraction in time for an initially slightly undersaturated magma (5 wt%). (c) Average eruption frequency (ky^{-1}) as a function of the inverse of the injection timescale, bulk compressibility, and critical overpressure. Dots are colored according to the number of phases present throughout the model simulation (2 = melt and crystals only; 3 = melt, crystals, and gas only; 2-3 = transition between two and three phases) (d) Average

eruption frequency as a function of the inverse of the cooling timescale, compressibility, and critical overpressure. Shaded triangles represent the volcanic systems of Laguna del Maule (L1 = Early post-glacial period; L2 = Holocene), Campi Flegrei (C1 = 1st epoch, C2 = 2nd epoch, C3 = 3rd epoch), Santorini (S1 = post-Minoan period, S2 = pre-Minoan), and Aso (A1 = Phase 1, and A2 = Phase 2). We use values of $\beta \sim 10^{-9}$ Pa^{-1} and $\Delta P_c \sim 20$ MPa for the volcanic systems.

We provide scaling relationships for eruption frequency that consider the combined effects of the mass recharge rate, initial chamber volume, and the average magma compressibility β. When mass recharge dominates the evolution of pressure ($\tau_{in} < \tau_{cool}$, Region 2 of Fig. 1), the eruption frequency f_{in} is inversely proportional to the injection timescale, the average bulk compressibility of the magma β, and the critical overpressure ΔP_c. When exsolution dominates the evolution of pressure ($\tau_{cool} < \tau_{in}$, Region 1 of Fig. 1), the eruption frequency f_{ex} is inversely proportional to the cooling timescale, β, and ΔP_c:

$$f_{in} = \frac{1}{\tau_{in}\beta\Delta P_c} \qquad (\tau_{in} < \tau_{cool}) \tag{5}$$

$$f_{ex} = \frac{1}{\tau_{cool}\beta\Delta P_c} \qquad (\tau_{in} > \tau_{cool}) \tag{6}$$

These scaling relationships are a good approximation of the model results (Fig. 2c and d). In addition, the trends in eruption frequencies for the various phases of volcanic activity at Santorini, Laguna del Maule, and Campi Flegrei are predicted moderately well by the scaling for the injection-dominated regime (Figure 2c). Aso Volcano is the only example that may be a better match to the scaling for eruptions triggered by second boiling (Figure 2d). On the other hand, uncertainties in estimated parameters or the assumption of identical β (10^{-9} Pa^{-1}) and ΔP_c (20 MPa) may cause a mismatch between scaling and observations. For example, if Aso Volcano has a greater volume fraction of MVPs than the other systems, β might be greater, shifting Aso left and closer to the scaling law for the injection-triggered regime.

Huppert and Woods (2002) provide a scaling relationship for the volume of a single eruption:

$$V_{er} = V\beta\Delta P_c \quad (7)$$

The good agreement between this scaling, the model results, and the eruption volume at silicic volcanic systems (Fig. 3) supports the validity of applying both the model and scaling to real systems. One useful application of these scaling laws is that we can potentially constrain the size and volatile saturation state of a magma chamber from the changes in eruption history. For example, consider the two eruptive phases of Laguna del Maule, the early post-glacial (E) and Holocene phases (H). During the early post-glacial phase, the eruption frequency was about 5.5 times greater and the eruptive volume was about 1/10 of what it was during the Holocene (Table 1). From the scaling for eruption frequency (eq. 5) and volume (eq. 7), and assuming the critical overpressure is unchanged, this implies:

$$\frac{f_{in,E}}{f_{in,H}} \sim \frac{\tau_{in,H}}{\tau_{in,E}} \frac{\beta_H}{\beta_E} \sim \frac{\dot{M}_{in,E} V_H}{\dot{M}_{in,H} V_E} \frac{\beta_H}{\beta_E} \sim 5.5 \quad (8)$$

$$\frac{V_{er,E}}{V_{er,H}} \sim \frac{V_E}{V_H} \frac{\beta_E}{\beta_H} \sim 0.1 \quad (9)$$

Substituting eq. (9) into eq. (8), we have

$$\frac{\dot{M}_{in,E}}{\dot{M}_{in,H}} \sim 0.55 \quad (10)$$

These relationships can be satisfied if the magma chamber during the Holocene was larger and more compressible than it was during the early post-glacial period, all of which would be true if the chamber grew and exsolved volatiles during the last ~25 ky. For example, if the exsolution of volatiles led to an increase in the compressibility by a factor of 5, the volume of the chamber must have grown by a factor of ~2.

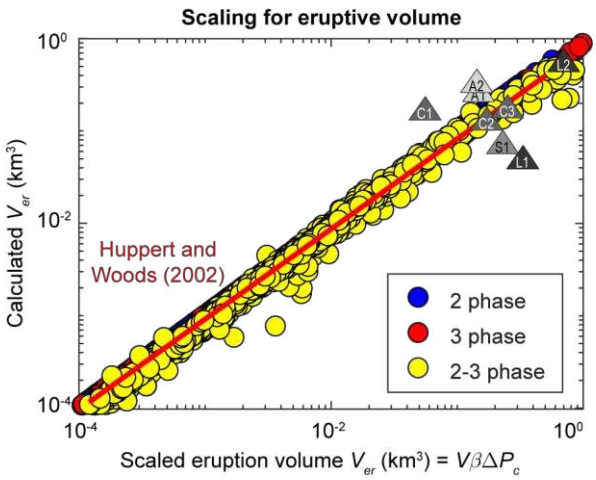

Figure 3. Average eruptive volume (per eruption) as a function of chamber volume V, compressibility β, and critical overpressure ΔP_c. Dots are colored according to the number of phases present throughout the model simulation (2 = melt and crystals only; 3 = melt, crystals, and gas only; 2-3 = transition between two and three phases). Red line represents the scaling for eruption volume (eq. 7) of Huppert and Woods (2002). Shaded triangles represent the volcanic systems of Laguna del Maule (L1 = Early post-glacial period; L2 = Holocene), Campi Flegrei (C1 = 1st epoch, C2 = 2nd epoch, C3 = 3rd epoch), Santorini (S1 = post-caldera period, S2 = pre-Minoan), and Aso (A1 = Phase 1, and A2 = Phase 2).

3.2.2 Ratio of mass erupted to mass added (M_{er}:M_{add}) *and chamber growth*

We calculate the total mass of magma erupted (summing over all eruptions) and supplied by recharge throughout the span of the model simulations (until crystal volume fraction reaches 50%). The balance between mass erupted / mass added (M_{er}:M_{add}; a rough proxy for the extrusive:intrusive ratio) provides insight on the overall growth of the magma chamber. Model results for M_{er}:M_{add} are plotted on regime diagrams for three different water concentrations (Figure 4). In the dry case (3 wt% water), almost none of the mass supplied by recharge is erupted, except within the injection-dominated regime (Region 2). Within this regime, M_{er}:M_{add} increases up and to the right, as the injection timescale decreases relative to the cooling and viscous relaxation timescales. In the wet case (5 wt% water), Regions 2 and 3 show a similar behavior to the dry case, with no eruptions occurring in Region 3 and so none of the mass leaving the chamber. However, the increased water content allows the possibility for eruption triggering by second boiling (Region 1). Within Region 1, we see that M_{er}:$M_{\text{add}} > 1$, indicating that there is significantly greater mass withdrawal during eruptions in this regime, such that magma chambers over time may actually shrink by mass. In Region 2, even though eruptions are

generally triggered by mass injection, we continue to see greater M_{er}:M_{add} for the wet case. In the intermediate case (4 wt% water), M_{er}:M_{add} is generally less than one across all regions, except for a few cases within Region 1 where eruptions are triggered by second boiling and significantly more mass is erupted than added. In Region 2, although M_{er}:M_{add} increases to the top-right as it does in the dry case, the values are overall intermediate between the dry and wet case (Figure 4).

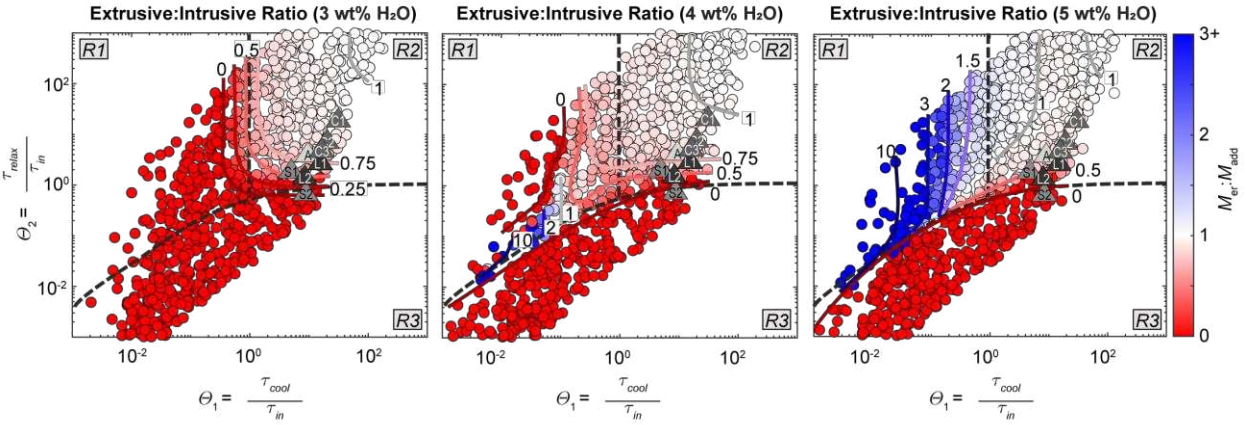

Figure 4. Ratio of the total mass erupted to added (by recharge), once the magma chamber reaches 50% crystal volume fraction, plotted for three different initial water concentrations. Red indicates growth, blue indicates shrinkage. Shaded triangles represent the volcanic systems of Laguna del Maule (L1 = Early post-glacial period; L2 = Holocene), Campi Flegrei (C1 = 1st epoch, C2 = 2nd epoch, C3 = 3rd epoch), Santorini (S1 = post-Minoan period, S2 = pre-Minoan), and Aso (A1 = Phase 1, and A2 = Phase 2).

While the extrusive:intrusive ratio M_{er}:M_{add} is famously difficult to quantify in real systems, it is generally believed to vary between ~ 0.1 – 0.5 (White et al., 2006) for upper crustal systems. Using values for θ_1 and θ_2 estimated for Laguna del Maule, Santorini, Campi Flegrei, and Aso, we see that all of these systems are expected to have M_{er}:M_{add} < 1. Of the systems we consider here, Laguna del Maule currently is the best constrained in terms of M_{er}:M_{add}, with an estimated ~8.4 km^3 erupted and 21.4 km^3 added (including erupted volume) over the Holocene, for a ratio of M_{er}:M_{add} = 0.4, which matches well with the predictions shown in Figure 4. In the regime space where the volcanic systems plot, M_{er}:M_{add} appears to be most sensitive to the value of θ_2, and does not appear to be very sensitive to water content (Fig. 4).

The overall effect on chamber growth of M_{er}:M_{add} can be viewed in terms of the change in mass and volume of the chamber (M_f/M_0 and V_f/V_0). In Figure 5, we show M_f/M_0 and V_f/V_0 on the regime diagrams for the wet, intermediate, and dry cases. In all three cases, growth by both mass and volume is enhanced to the bottom-right of the regime diagrams, where θ_1 is large while θ_2 is

small. This "zone of efficient growth" occurs where greater mass recharge leads to short injection timescales, but where the relaxation timescale is comparable to the injection timescale, allowing growth by crustal deformation. This zone straddles the boundary between Region 2, in which many eruptions take place (Fig. 1), and Region 3, in which no eruptions take place (Fig.1). In other words, the model results indicate that growth can occur with or without eruptions. Using values for θ_1 and θ_2 estimated for Laguna del Maule, Santorini, Campi Flegrei, and Aso, we find that almost all of the volcanic systems fall within the "zone of efficient growth" overlapping Region 2, where eruptions occur and are dominated by injection (Fig. 5). Only the values for Santorini prior to the Minoan eruption fall within Region 3, but close to the boundary with Region 2. For all of these systems, model results predict growth by both mass and volume during eruptive phases, as seems to be occurring in nature.

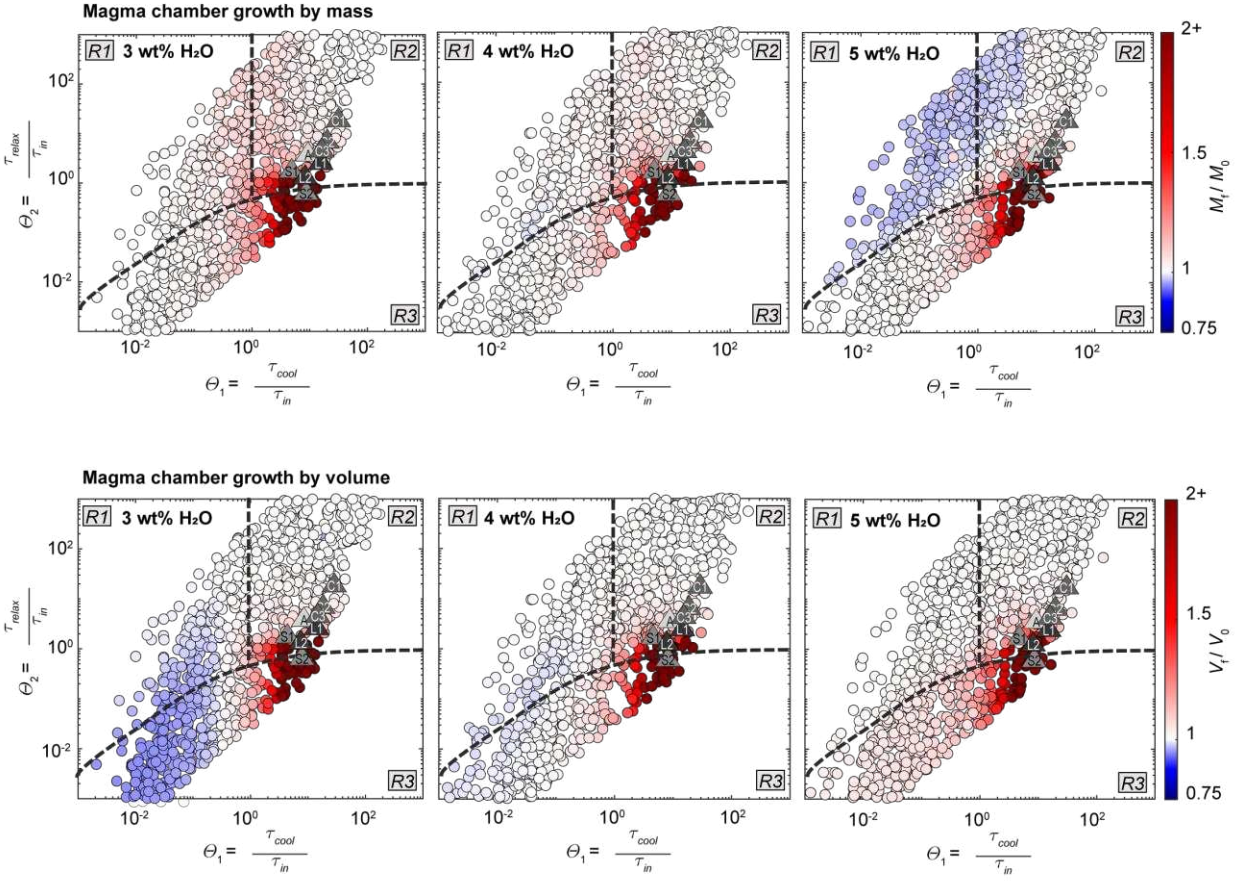

Figure 5. Chamber growth by mass M_f / M_0 (upper panels) and volume V_f / V_0 (lower panels), for three different parental water concentrations. Red indicates growth, while blue indicates shrinkage. Shaded triangles represent volcanic phases from Laguna del Maule (L1 = Early post-glacial period; L2 = Holocene), Campi Flegrei (C1 = 1st

epoch, C2 = 2nd epoch, C3 = 3rd epoch), Santorini (S1 = post-Minoan period, S2 = pre-Minoan), and Aso (A1 = Phase 1, and A2 = Phase 2).

Model results show that chamber growth by volume follows a different trend than growth by mass. Although in the wet case we see mass loss where eruptions are triggered by second boiling, the volumes of the chambers remain constant because of the exsolution of the low-density MVP. In the dry case, in Regions 1 and 3 for which $\tau_{cool} < \tau_{in}$ and no eruptions occur, crystallization increases the bulk density and the volume of the chamber shrinks (Fig. 5d).

One of the outstanding questions in volcanology is how long it takes for chambers to build up to the caldera stage, and what governs this timescale. From the model results, we calculated volumetric growth rates by averaging the changes in chamber volume over the duration of the model simulation, i.e. until $\epsilon_x = 50\%$ (Figure 6). We find that the growth rate varies by over 5 orders of magnitude across the regime diagrams, increasing to the bottom right from ~10^{-7} km^3/yr where θ_2 is large and θ_1 is small, up to ~10^{-2} km^3/yr where θ_2 is small while θ_1 is large. There are no significant differences in growth rates as a function of water content, except where $\theta_1 < 1$ and no growth is possible for the dry cases. The volcanic systems of interest all tend to plot along a contour of similar growth rate equal to about 10^{-3} km^3/yr (Figure 6).

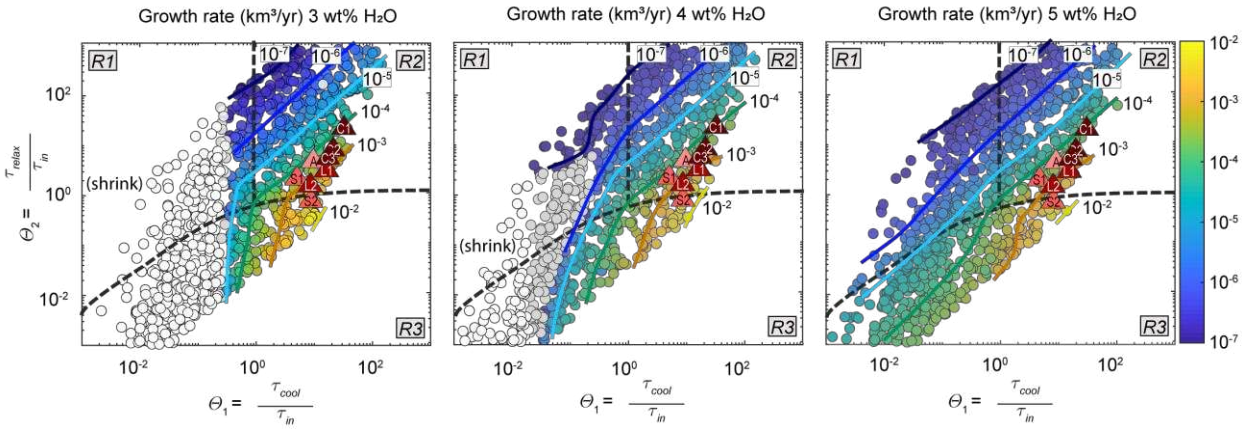

Figure 6. Growth rates calculated from model results, in km^3/yr. White points refer to cases where volume either shrinks or remains constant. Shaded triangles represent the volcanic systems of Laguna del Maule (L1 = Early post-glacial period; L2 = Holocene), Campi Flegrei (C1 = 1st epoch, C2 = 2nd epoch, C3 = 3rd epoch), Santorini (S1 = post-Minoan period, S2 = pre-Minoan), and Aso (A1 = Phase 1, and A2 = Phase 2).

4. Discussion

4.1 Interplay of extrusive:intrusive ratio, eruption frequency, and chamber growth

At the most basic level, magma chambers will grow when M_{er}:M_{add} < 1 and shrink when M_{er}:M_{add} > 1, but why shouldn't the mass of magma erupted simply equal the mass of magma added? Divergence from M_{er}:M_{add} = 1 occurs when irreversible processes – viscous relaxation and phase changes during cooling – change how fast pressure can build or drop between and during eruptions. This can be understood better by considering the change in chamber pressure resulting from mass inflow and eruption:

$$\beta \frac{dP}{dt} = \frac{\dot{M}_{in} - \dot{M}_{out}}{\rho V} - \frac{\Delta P}{\eta_r} \quad (11)$$

where the last term accounts for viscous relaxation of the crust and $\Delta P = P(t) - P_{lit}$. If we integrate over a single eruption cycle and decompose the pressure evolution into the period between and during the eruption, we find the total change in mass of the chamber during one eruption cycle:

$$\Delta M = \int_{repose} \rho V \beta \frac{dP}{dt} dt + \int_{eruption} \rho V \beta \frac{dP}{dt} dt + \int_{repose} \frac{\rho V \Delta P}{\eta_r} dt + \int_{eruption} \frac{\rho V \Delta P}{\eta_r} dt \quad (12)$$

The viscous response during the eruption can be neglected because the eruption duration is small compared to the repose time (1/*f*):

$$\Delta M \approx \langle \rho V \beta \rangle_{repose} \Delta P_c - \langle \rho V \beta \rangle_{eruption} \Delta P_c + \langle \rho V {\eta_r}^{-1} \rangle_{repose} \Delta P f^{-1} \quad (13)$$

where $\langle \rho V \beta \rangle$ indicates the average values of magma density, chamber volume, and magma compressibility during the repose or eruption phase. From eq. (13), we can see one way in which eruption frequency affects chamber growth; a longer repose time (lower eruption frequency) allows greater mass accumulation by viscous deformation of the crust. If viscous

relaxation dominates, for example in Region 3 where no eruptions occur and the second term is zero (Fig. 1), magma recharge always leads to chamber growth.

It is possible for a magma chamber being constantly recharged to shrink. If eruption frequency is high or if η_r is very large (e.g. Regions 1 and 2 where $\theta_2 > 10$, Fig. 1), the viscous term in eq. (13) may be neglected and a chamber will shrink by mass if $\langle \rho V \beta \rangle_{eruption} > \langle \rho V \beta \rangle_{repose}$. Between eruptions, cooling and crystallization leads to second boiling, which increases the value of β (eq. 4) such that it takes on a greater value at the initiation of an eruption and $\langle \rho V \beta \rangle_{eruption} > \langle \rho V \beta \rangle_{repose}$. As a result, the mass lost during the eruption is greater than the mass added during repose and the chamber shrinks, a result that is consistent with previous work on the effect of volatiles on eruption size and frequency (Bower & Woods, 1997; Huppert & Woods, 2002; Woods & Huppert, 2003). As eruption frequency increases and there is less time between eruptions for second boiling (θ_1 increasing), the discrepancy between $\langle \rho V \beta \rangle_{repose}$ and $\langle \rho V \beta \rangle_{eruption}$ decreases and the mass balance approaches a neutral budget, i.e. less shrinking occurs (Fig. 5c).

A key distinction we draw from the numerical results is the difference between growth by mass and volume. While a non-eruptive chamber will always grow by mass when supplied with magma, if the cooling rate outpaces injection ($\tau_{cool} < \tau_{in}$), crystallization and volatile exsolution can change the bulk density of the magma. In dry cases (e.g. Fig. 5a and d), crystallization dominates and the density increases, leading to volumetric shrinkage. In sufficiently wet systems (e.g. Fig. 5c and f), exsolution balances this and the volume can remain constant or even increase.

Overall, growth by both mass and volume is favored when injection and crustal relaxation are both fast compared to cooling, highlighted by a zone in the bottom-right of the regime space spanning ~$\theta_1 = 1 - 50$ and ~$\theta_2 = 0.05 - 5$ (Figure 7a). Within this "zone of efficient growth", growth is rapid and appears to be decoupled from eruption frequency, as it intersects both Region 2, where hundreds or more eruptions can occur before the chamber freezes, and Region 3 where no eruptions are expected to occur (Fig. 1). In other words, there is a narrow zone where magma recharge is just faster than relaxation but much faster than cooling, where chambers can simultaneously erupt and grow. The values of θ_1 and θ_2 estimated for the volcanic epochs of Laguna del Maule, Campi Flegrei, post-caldera Santorini, and Aso all plot within this zone of simultaneous eruption and growth, suggesting that during flare-ups of

volcanic activity, the underlying chambers are actually growing (Fig. 7). The pre-Minoan magma chamber at Santorini falls in Region 3 (no eruptions expected) primarily due to its large size (~50 km^3), suggesting that the Minoan eruption may have been triggered by a shift towards greater magma recharge rates leading up to the eruption (Druitt et al., 2012).

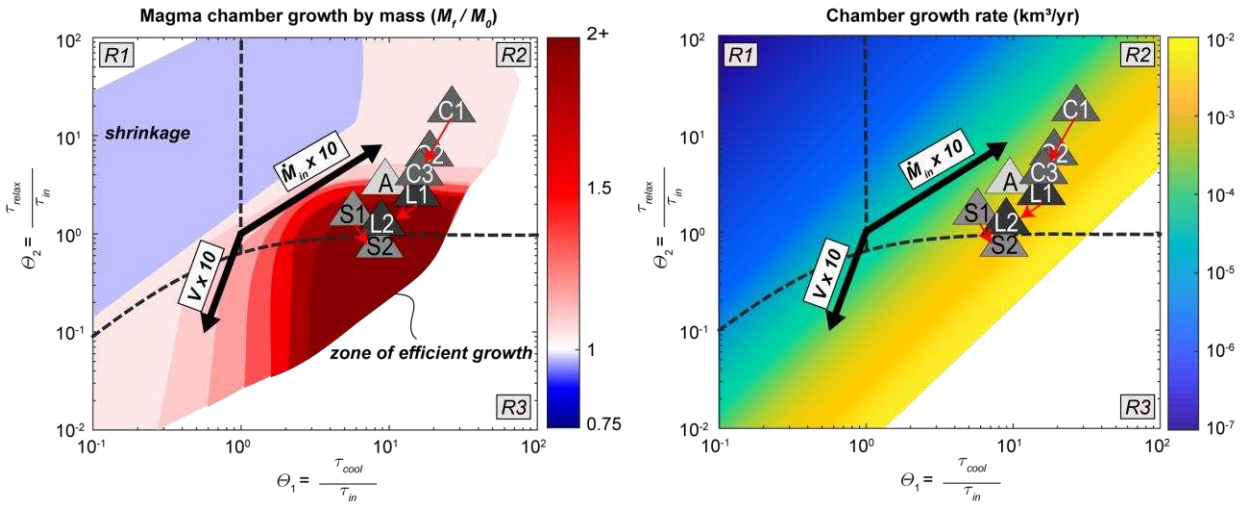

Figure 7. Trajectories of θ_1 and θ_2 in regime space taken as chambers progress along the caldera cycle. Bold black arrows provide an "uncertainty" related to model parameters: the length and direction of the arrows indicate how a system would shift in regime space if the chamber volume or mass inflow rate were different by one order of magnitude. Left panel: Magma chamber growth by mass, for 5 wt% water. Right panel: Chamber growth rates, for 5 wt% water. Shaded triangles represent the volcanic systems of Laguna del Maule (L1 = Early post-glacial period; L2 = Holocene), Campi Flegrei (C1 = 1st epoch, C2 = 2nd epoch, C3 = 3rd epoch), Santorini (S1 = post-Minoan period, S2 = pre-Minoan), and Aso (A1 = Phase 1, and A2 = Phase 2).

4.2 How do small chambers grow?

The model results suggest that growth is favored by larger chambers, and that smaller chambers will erupt frequently and grow more slowly. We explore how small chambers grow to the sizes required to produce massive caldera-forming eruptions by considering how the timescales for injection, cooling, and viscous relaxation evolve during growth. The non-dimensional quantities θ_1 and θ_2 are defined by the initial conditions of the magma chamber. In fact, these quantities evolve as the chamber grows, and in real systems they would further evolve as mass supply rate fluctuates and as the temperature of the host rock evolves (Karakas, Degruyter, Bachmann, & Dufek, 2017). In the regime space, growth of the chamber would cause θ_1 to decrease as $V^{-1/3}$ and θ_2 to decrease as V^{-1}, represented by one of the bold arrows in Figure

7. As the chamber grows and moves along this trajectory, it moves toward regions in which growth is encouraged and growth rates increase (Fig.7b). This suggests that the chamber volume should increase nonlinearly in time, growing faster as the chamber gets larger (Fig. 8). In addition, this implies that over time, even though eruptions should increase in size because of a larger chamber, the ratio of magma erupted to added will decrease overall.

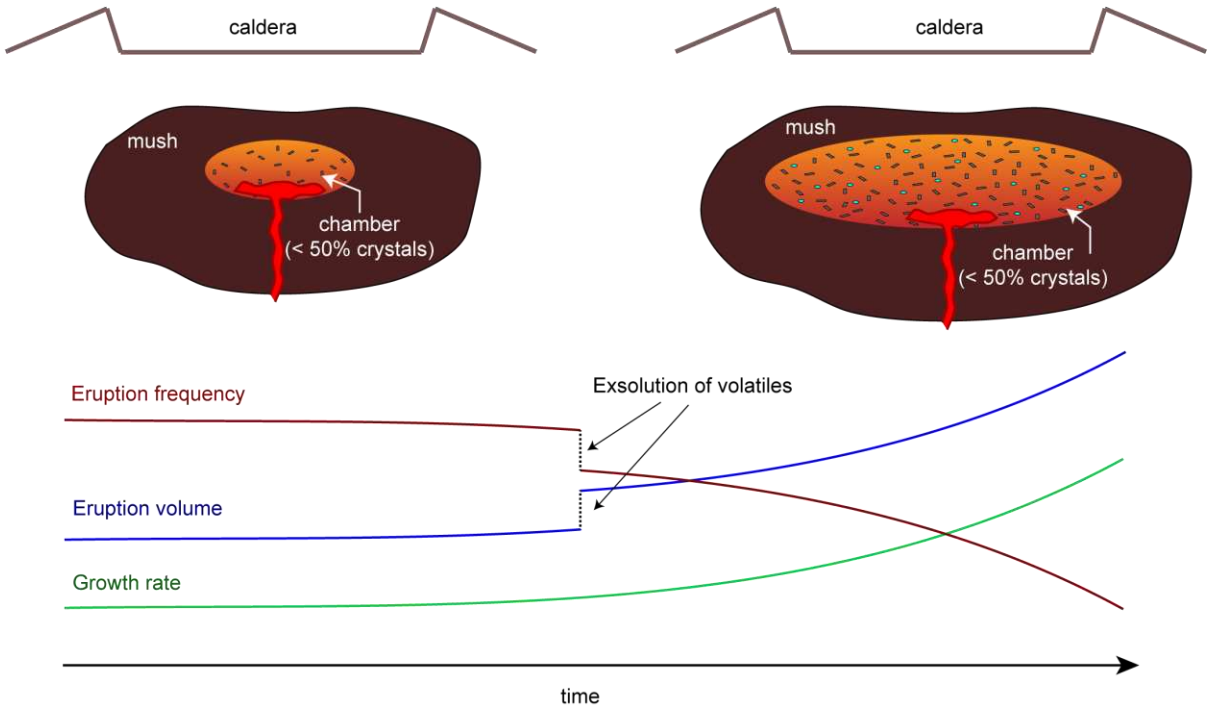

Figure 8. Conceptual model for the growth of subvolcanic magma chambers during inter-caldera periods, and associated changes in eruption frequency and volume. When magma chambers are small, eruptions are relatively frequent but small in volume, and the rate of growth of the chamber is slow but positive. Eventually as the chamber increases in size, growth rates increase, and eruptions become larger and less frequent. Exsolution of volatiles results in an increase of magma compressibility, suppressing eruption frequency and encouraging larger-volume eruptions.

The volcanic systems of Laguna del Maule, Campi Flegrei, and to some extent Santorini all evolve along the trajectory of increasing volume during inter-caldera periods (Fig. 7). For example, the eruptible portion of the Campi Flegrei magma reservoir during Epoch 1 ("C1" in Fig. 7) is inferred to have been relatively small (~2.5 km^3) compared to the sizes of its largest eruptions (~40 and 300 km^3). According to the model results presented here, growth during this time may have been as slow as ~$3*10^{-4}$ km^3/yr, which if kept constant (assuming an effective average mass recharge) would add ~2 km^3 to the chamber by the time of Epoch 2 ~6000 years later. By Epoch 3, however, the chamber was larger and the growth rate may have been as fast as

~10^{-3} km^3/yr. At that rate, it would take ~30,000 years to grow to the size of the Neapolitan Yellow Tuff, which is roughly the amount of time between the eruptions of the two most recent caldera-forming eruptions of the Campanian Ignimbrite and the Neapolitan Yellow Tuff.

We note, however, that the initial size and magma supply rates of the Campi Flegrei system during Epoch 1 place it within the regime space where growth already is favored (Fig. 7a). For magma chambers initially much smaller than ~1 km^3, growth is not expected to be significant and the trajectory through the regime space due to changes in volume would be much smaller than the trajectories illustrated by the volcanic systems presented here. In order for very small systems (< 1 km^3) to move toward conditions favorable for growth, another mechanism may be required, such as a decrease in the host-rock viscosity, which would shift the trajectory vertically down towards regions of increased growth. In reality, growth during the incipient stages of chamber formation is probably encouraged by some combination of increasing magma supply rates and decreasing host-rock viscosity as the crust warms up, and these processes are important targets for future research. From the analysis presented here, we hypothesize that while growth may be limited in the early stages of chamber formation, if a chamber reaches a critical volume (in this model ~1 km^3), growth becomes encouraged and the rate of growth can speed up over time (Fig. 8).

6. Conclusions

Deposits from long-lived, caldera-forming volcanic systems such as Laguna del Maule, Campi Flegrei, Santorini, and Aso suggest that silicic magma chambers can grow from a few km^3 to hundreds of km^3 or more in the span of tens to hundreds of thousands of years. Here we use a thermo-mechanical magma chamber model to examine conditions that would promote the growth of these systems from the post- to pre-caldera stage. We find that growth is optimized when the timescale for magma injection is short compared to the timescale for chamber cooling ($\theta_1 > 1$), and when the timescale for viscous relaxation of the crust is comparable to the timescale for injection ($\theta_2 \sim 1$). Within this "zone of efficient growth," if the viscous relaxation timescale is just shorter than the injection timescale ($\theta_2 < 1$), no eruptions occur and all magma supplied to the system is stored within the chamber. If the viscous relaxation timescale is just longer than the injection timescale ($\theta_2 > 1$), growth is accompanied by multiple volcanic

eruptions, which is expected to be the case for Laguna del Maule, Campi Flegrei, Santorini, and Aso. We interpret this to mean that flare-ups in volcanic activity during inter-caldera periods at these volcanoes may actually signal growth of the underlying chamber.

In summary, growth rates may initially be slow (~10^{-4} km^3/yr), when magma chambers are small (~1 km^3), but as the chamber grows, this rate increases nonlinearly (Fig. 8). For systems that both grow and erupt, chamber growth corresponds to changes in the frequency and size of volcanic eruptions, such that frequency decreases and eruption volume increases in proportion with chamber volume (Fig. 8). In addition, exsolution of magmatic volatiles can increase the bulk compressibility of the magma, leading to proportional decreases in eruption frequency and increases in eruption volume (Fig. 8). Altogether, the scaling for eruption frequency and eruption volume as a function of chamber volume, magma supply rate, and magma compressibility (state of volatile saturation) compare well with observations from Laguna del Maule, Campi Flegrei, Santorini, and Aso, which supports the use of the volcanic record to probe conditions and growth rates of underlying magma chambers.

Acknowledgements

Funding for this research was provided in part by grants from the National Science Foundation, NSF EAR (1760004) to Townsend and Huber, NSF Integrated Earth System EAR (1411724) to Huber. Bachmann acknowledges support from Swiss SNF grant # 200021_178928. All data from the volcanic systems come from published literature and are included in Table 2. Please refer to the supporting information for the input and output files for all model simulations.

References

Andersen, N. L., Singer, B. S., Costa, F., Fournelle, J., Herrin, J. S., & Fabbro, G. N. (2018). Petrochronologic perspective on rhyolite volcano unrest at Laguna del Maule, Chile. *Earth and Planetary Science Letters, 493*, 57-70. doi:10.1016/j.epsl.2018.03.043

Andersen, N. L., Singer, B. S., Jicha, B. R., Beard, B. L., Johnson, C. M., & Licciardi, J. M. (2017). Pleistocene to Holocene Growth of a Large Upper Crustal Rhyolitic Magma Reservoir beneath the Active Laguna del Maule Volcanic Field, Central Chile. *Journal of Petrology, 58*(1), 85-114. doi:10.1093/petrology/egx006

Annen, C. (2009). From plutons to magma chambers: Thermal constraints on the accumulation of eruptible silicic magma in the upper crust. *Earth and Planetary Science Letters, 284*(3-4), 409-416. doi:10.1016/j.epsl.2009.05.006

Barton, M., & Huijsmans, J. P. P. (1986). Post-caldera dacites from the Santorini volcanic complex, Aegean Sea, Greece -- an examples of the eruption of lavas of near-constant composition over a 2,200 year period. *Contributions to Mineralogy and Petrology, 94*(4), 472-495. doi:10.1007/bf00376340

Bevilacqua, A., Bursik, M., Patra, A., Pitman, E. B., Yang, Q. Y., Sangani, R., & Kobs-Nawotniak, S. (2018). Late Quaternary Eruption Record and Probability of Future Volcanic Eruptions in the Long Valley Volcanic Region (CA, USA). *Journal of Geophysical Research-Solid Earth, 123*(7), 5466-5494. doi:10.1029/2018jb015644

Bevilacqua, A., Flandoli, F., Neri, A., Isaia, R., & Vitale, S. (2016). Temporal models for the episodic volcanism of Campi Flegrei caldera (Italy) with uncertainty quantification. *Journal of Geophysical Research-Solid Earth, 121*(11), 7821-7845. doi:10.1002/2016jb013171

Black, B. A., & Manga, M. (2016). The eruptibility of magmas at Tharsis and Syrtis Major on Mars. *Journal of Geophysical Research-Planets, 121*(6), 944-964. doi:10.1002/2016je004998

Black, B. A., & Manga, M. (2017). Volatiles and the tempo of flood basalt magmatism. *Earth and Planetary Science Letters, 458*, 130-140. doi:10.1016/j.epsl.2016.09.035

Blake, S. (1984). Volatile oversaturation during the evolution of silicic magma chambers as an eruption trigger. *Journal of Geophysical Research, 89*(NB10), 8237-8244. doi:10.1029/JB089iB10p08237

Bower, S. M., & Woods, A. W. (1997). Control of magma volatile content and chamber depth on the mass erupted during explosive volcanic eruptions. *Journal of Geophysical Research-Solid Earth, 102*(B5), 10273-10290. doi:10.1029/96jb03176

Cadoux, A., Scaillet, B., Druitt, T. H., & Deloule, E. (2014). Magma Storage Conditions of Large Plinian Eruptions of Santorini Volcano (Greece). *Journal of Petrology, 55*(6), 1129-1171. doi:10.1093/petrology/egu021

Calo, M., & Tramelli, A. (2018). Anatomy of the Campi Flegrei caldera using Enhanced Seismic Tomography Models. *Scientific Reports, 8*. doi:10.1038/s41598-018-34456-x

Caricchi, L., Annen, C., Blundy, J., Simpson, G., & Pinel, V. (2014). Frequency and magnitude of volcanic eruptions controlled by magma injection and buoyancy. *Nature Geoscience, 7*(2), 126-130. doi:10.1038/ngeo2041

Chamberlain, K. J., Wilson, C. J. N., Wooden, J. L., Charlier, B. L. A., & Ireland, T. R. (2014). New Perspectives on the Bishop Tuff from Zircon Textures, Ages and Trace Elements. *Journal of Petrology, 55*(2), 395-426. doi:10.1093/petrology/egt072

Charlier, B. L. A., Wilson, C. J. N., & Davidson, J. P. (2008). Rapid open-system assembly of a large silicic magma body: time-resolved evidence from cored plagioclase crystals in the Oruanui eruption deposits, New Zealand. *Contributions to Mineralogy and Petrology, 156*(6), 799-813. doi:10.1007/s00410-008-0316-y

Christiansen, R. L. (2001). *The Quaternary and Pliocene Yellowstone Plateau Volcanic Field of Wyoming, Idaho, and Montana*. U.S. Geological Survey Professional Paper.

Cottrell, E., Gardner, J. E., & Rutherford, M. J. (1999). Petrologic and experimental evidence for the movement and heating of the pre-eruptive Minoan rhyodacite (Santorini, Greece). *Contributions to Mineralogy and Petrology, 135*(4), 315-331. doi:10.1007/s004100050514

de Silva, S. L., & Gregg, P. M. (2014). Thermomechanical feedbacks in magmatic systems: Implications for growth, longevity, and evolution of large caldera-forming magma

reservoirs and their supereruptions. *Journal of Volcanology and Geothermal Research, 282*, 77-91. doi:10.1016/j.jvolgeores.2014.06.001

Degruyter, W., & Huber, C. (2014). A model for eruption frequency of upper crustal silicic magma chambers. *Earth and Planetary Science Letters, 403*, 117-130. doi:10.1016/j.epsl.2014.06.047

Degruyter, W., Huber, C., Bachmann, O., Cooper, K. M., & Kent, A. J. R. (2016). Magma reservoir response to transient recharge events: The case of Santorini volcano (Greece). *Geology, 44*(1), 23-26. doi:10.1130/g37333.1

Degruyter, W., Huber, C., Bachmann, O., Cooper, K. M., & Kent, A. J. R. (2017). Influence of Exsolved Volatiles on Reheating Silicic Magmas by Recharge and Consequences for Eruptive Style at Volcan Quizapu (Chile). *Geochemistry Geophysics Geosystems, 18*(11), 4123-4135. doi:10.1002/2017gc007219

Deino, A. L., Orsi, G., de Vita, S., & Piochi, M. (2004). The age of the Neapolitan Yellow Tuff caldera-forming eruption (Campi Flegrei caldera Italy) assessed by Ar-40/Ar-39 dating method. *Journal of Volcanology and Geothermal Research, 133*(1-4), 157-170. doi:10.1016/s0377-0273(03)00396-2

Del Negro, C., Currenti, G., & Scandura, D. (2009). Temperature-dependent viscoelastic modeling of ground deformation: Application to Etna volcano during the 1993-1997 inflation period. *Physics of the Earth and Planetary Interiors, 172*(3-4), 299-309. doi:10.1016/j.pepi.2008.10.019

Di Vito, M. A., Acocella, V., Aiello, G., Barra, D., Battaglia, M., Carandente, A., . . . Terrasi, F. (2016). Magma transfer at Campi Flegrei caldera (Italy) before the 1538 AD eruption. *Scientific Reports, 6*. doi:10.1038/srep32245

Di Vito, M. A., Isaia, R., Orsi, G., Southon, J., de Vita, S., D'Antonio, M., . . . Piochi, M. (1999). Volcanism and deformation since 12,000 years at the Campi Flegrei caldera (Italy). *Journal of Volcanology and Geothermal Research, 91*(2-4), 221-246. doi:10.1016/s0377-0273(99)00037-2

Dragoni, M., & Magnanensi, C. (1989). Displacement and stress produced by a pressurized, spherical magma chamber, surrounded by a viscoelastic shell. *Physics of the Earth and Planetary Interiors, 56*(3-4), 316-328. doi:10.1016/0031-9201(89)90166-0

Druitt, T. H., Costa, F., Deloule, E., Dungan, M., & Scaillet, B. (2012). Decadal to monthly timescales of magma transfer and reservoir growth at a caldera volcano. *Nature, 482*(7383), 77-U97. doi:10.1038/nature10706

Druitt, T. H., & Francaviglia, V. (1992). Caldera formation on Santorini and the physiography of the islands in the Late Bronze Age. *Bulletin of Volcanology, 54*(6), 484-493. doi:10.1007/bf00301394

Druitt, T. H., Mellors, R. A., Pyle, D. M., & Sparks, R. S. J. (1989). Explosive volcanism on Santorini, Greece. *Geological Magazine, 126*(2), 95-126. doi:10.1017/s0016756800006270

Druitt, T. H., Mercier, M., Florentin, L., Deloule, E., Cluzel, N., Flaherty, T., . . . Cadoux, A. (2016). Magma Storage and Extraction Associated with Plinian and Interplinian Activity at Santorini Caldera (Greece). *Journal of Petrology, 57*(3), 461-494. doi:10.1093/petrology/egw015

Dufek, J., & Bergantz, G. W. (2005). Transient two-dimensional dynamics in the upper conduit of a rhyolitic eruption: A comparison of closure models for the granular stress. *Journal of*

824 *Volcanology and Geothermal Research, 143*(1-3), 113-132.
825 doi:10.1016/j.jvolgeores.2004.09.013
826 Fedi, M., Cella, F., D'Antonio, M., Florio, G., Paoletti, V., & Morra, V. (2018). Gravity
827 modeling finds a large magma body in the deep crust below the Gulf of Naples, Italy.
828 *Scientific Reports, 8*. doi:10.1038/s41598-018-26346-z
829 Feigl, K. L., Le Mevel, H., Ali, S. T., Cordova, L., Andersen, N. L., DeMets, C., & Singer, B. S.
830 (2014). Rapid uplift in Laguna del Maule volcanic field of the Andean Southern Volcanic
831 zone (Chile) 2007-2012. *Geophysical Journal International, 196*(2), 885-901.
832 doi:10.1093/gji/ggt438
833 Flaherty, T., Druitt, T. H., Tuffen, H., Higgins, M. D., Costa, F., & Cadoux, A. (2018). Multiple
834 timescale constraints for high-flux magma chamber assembly prior to the Late Bronze
835 Age eruption of Santorini (Greece). *Contributions to Mineralogy and Petrology, 173*(9).
836 doi:10.1007/s00410-018-1490-1
837 Forni, F., Degruyter, W., Bachmann, O., De Astis, G., & Mollo, S. (2018). Long-term magmatic
838 evolution reveals the beginning of a new caldera cycle at Campi Flegrei. *Science*
839 *Advances, 4*(11). doi:10.1126/sciadv.aat9401
840 Gelman, S. E., Gutierrez, F. J., & Bachmann, O. (2013). On the longevity of large upper crustal
841 silicic magma reservoirs. *Geology, 41*(7), 759-762. doi:10.1130/g34241.1
842 Hata, M., Matsushima, N., Takakura, S., Utsugi, M., Hashimoto, T., & Uyeshima, M. (2018).
843 Three-dimensional electrical resistivity modeling to elucidate the crustal magma supply
844 system beneath Aso caldera, Japan. *Journal of Geophysical Research: Solid Earth, 123*.
845 doi:10.102 9/2018JB015951
846 Hata, M., Takakura, S., Matsushima, N., Hashimoto, T., & Utsugi, M. (2016). Crustal magma
847 pathway beneath Aso caldera inferred from three-dimensional electrical resistivity
848 structure. *Geophysical Research Letters, 43*(20), 10720-10727.
849 doi:10.1002/2016gl070315
850 Hildreth, W. (1981). Gradients in silicic magma chambers -- implications for lithospheric
851 magmatism. *Journal of Geophysical Research, 86*(NB11), 153-192.
852 doi:10.1029/JB086iB11p10153
853 Hildreth, W., Godoy, E., Fierstein, J., & Singer, B. (2010). Laguna del Maule Volcanic Field:
854 Eruptive history of a Quaternary basalt-to-rhyolite distributed volcanic field on the
855 Andean rangecrest in central Chile. *Servicio Nacional de Geologia y Mineria -- Chile, 63*.
856 Huber, C., Bachmann, O., & Manga, M. (2009). Homogenization processes in silicic magma
857 chambers by stirring and mushification (latent heat buffering). *Earth and Planetary*
858 *Science Letters, 283*(1-4), 38-47. doi:10.1016/j.epsl.2009.03.029
859 Huppert, H. E., & Woods, A. W. (2002). The role of volatiles in magma chamber dynamics.
860 *Nature, 420*(6915), 493-495. doi:10.1038/nature01211
861 Jellinek, A. M., & DePaolo, D. J. (2003). A model for the origin of large silicic magma
862 chambers: precursors of caldera-forming eruptions. *Bulletin of Volcanology, 65*(5), 363-
863 381. doi:10.1007/s00445-003-0277-y
864 Johnston, E. N., Sparks, R. S. J., Phillips, J. C., & Carey, S. (2014). Revised estimates for the
865 volume of the Late Bronze Age Minoan eruption, Santorini, Greece. *Journal of the*
866 *Geological Society, 171*(4), 583-590. doi:10.1144/jgs2013-113
867 Kaneko, K., Kamata, H., Koyaguchi, T., Yoshikawa, M., & Furukawa, K. (2007). Repeated
868 large-scale eruptions from a single compositionally stratified magma chamber: An

example from Aso volcano, Southwest Japan. *Journal of Volcanology and Geothermal Research, 167*(1-4), 160-180. doi:10.1016/j.jvolgeores.2007.05.002

Karakas, O., Degruyter, W., Bachmann, O., & Dufek, J. (2017). Lifetime and size of shallow magma bodies controlled by crustal-scale magmatism. *Nature Geoscience, 10*(6), 446-+. doi:10.1038/ngeo2959

Karlstrom, L., Dufek, J., & Manga, M. (2009). Organization of volcanic plumbing through magmatic lensing by magma chambers and volcanic loads. *Journal of Geophysical Research-Solid Earth, 114*. doi:10.1029/2009jb006339

Karlstrom, L., Dufek, J., & Manga, M. (2010). Magma chamber stability in arc and continental crust. *Journal of Volcanology and Geothermal Research, 190*(3-4), 249-270. doi:10.1016/j.jvolgeores.2009.10.003

Le Mevel, H., Gregg, P. M., & Feigl, K. L. (2016). Magma injection into a long-lived reservoir to explain geodetically measured uplift: Application to the 2007-2014 unrest episode at Laguna del Maule volcanic field, Chile. *Journal of Geophysical Research-Solid Earth, 121*(8), 6092-6108. doi:10.1002/2016jb013066

Lipman, P. W., Steven, T. A., & Mehnert, H. H. (1970). Volcanic history of San-Juan-Mountains, Colorado, as indicated by potassium-argon dating. *Geological Society of America Bulletin, 81*(8), 2329-&. doi:10.1130/0016-7606(1970)81[2329:vhotsj]2.0.co;2

Magee, C., Stevenson, C. T. E., Ebmeier, S. K., Keir, D., Hammond, J. O. S., Gottsmann, J. H., . . . Jackson, M. D. (2018). Magma Plumbing Systems: A Geophysical Perspective. *Journal of Petrology, 59*(6), 1217-1251. doi:10.1093/petrology/egy064

Matthews, N. E., Vazquez, J. A., & Calvert, A. T. (2015). Age of the Lava Creek supereruption and magma chamber assembly at Yellowstone based on Ar-40/Ar-39 and U-Pb dating of sanidine and zircon crystals. *Geochemistry Geophysics Geosystems, 16*(8), 2508-2528. doi:10.1002/2015gc005881

McKee, C. O., Lowenstein, P. L., De Saint Ours, P., Talai, B., Itikarai, I., & Mori, J. J. (1984). Seismic and ground deformation crises at Rabaul Caldera: Prelude to an eruption? *Bulletin of Volcanology, 47*(2), 397-411.

Miller, C. A., Williams-Jones, G., Fournier, D., & Witter, J. (2017). 3D gravity inversion and thermodynamic modelling reveal properties of shallow silicic magma reservoir beneath Laguna del Maule, Chile. *Earth and Planetary Science Letters, 459*, 14-27. doi:10.1016/j.epsl.2016.11.007

Miller, C. F., Furbish, D. J., Walker, B. A., Claiborne, L. L., Koteas, G. C., Bleick, H. A., & Miller, J. S. (2011). Growth of plutons by incremental emplacement of sheets in crystal-rich host: Evidence from Miocene intrusions of the Colorado River region, Nevada, USA. *Tectonophysics, 500*(1-4), 65-77. doi:10.1016/j.tecto.2009.07.011

Miller, R. B., & Paterson, S. R. (2001). Construction of mid-crustal sheeted plutons: Examples from the north Cascades, Washington. *Geological Society of America Bulletin, 113*(11), 1423-1442. doi:10.1130/0016-7606(2001)113<1423:comcsp>2.0.co;2

Miyabuchi, Y. (2009). A 90,000-year tephrostratigraphic framework of Aso Volcano, Japan. *Sedimentary Geology, 220*(3-4), 169-189. doi:10.1016/j.sedgeo.2009.04.018

Miyoshi, M., Sumino, H., Miyabuchi, Y., Shinmura, T., Mori, Y., Hasenaka, T., . . . Nagao, K. (2012). K-Ar ages determined for post-caldera volcanic products from Aso volcano, central Kyushu, Japan. *Journal of Volcanology and Geothermal Research, 229*, 64-73. doi:10.1016/j.jvolgeores.2012.04.003

Newman, A. V., Dixon, T. H., & Gourmelen, N. (2006). A four-dimensional viscoelastic deformation model for Long Valley Caldera, California, between 1995 and 2000. *Journal of Volcanology and Geothermal Research, 150*(1-3), 244-269. doi:10.1016/j.jvolgeores.2005.07.017

Orsi, G., DeVita, S., & diVito, M. (1996). The restless, resurgent Campi Flegrei nested caldera (Italy): Constraints on its evolution and configuration. *Journal of Volcanology and Geothermal Research, 74*(3-4), 179-214. doi:10.1016/s0377-0273(96)00063-7

Orsi, G., Di Vito, M. A., & Isaia, R. (2004). Volcanic hazard assessment at the restless Campi Flegrei caldera. *Bulletin of Volcanology, 66*(6), 514-530. doi:10.1007/s00445-003-0336-4

Papadopoulos, G. A., Sachpazi, M., Panopoulou, G., & Stavrakakis, G. (1998). The volcanoseismic crisis of 1996-97 in Nisyros, SE Aegean Sea, Greece. *Terra Nova, 10*(3), 151-154.

Parks, M. M., Biggs, J., England, P., Mather, T. A., Nomikou, P., Palamartchouk, K., . . . Zacharis, V. (2012). Evolution of Santorini Volcano dominated by episodic and rapid fluxes of melt from depth. *Nature Geoscience, 5*(10), 749-754. doi:10.1038/ngeo1562

Paterson, S. R., & Miller, R. B. (1998). Mid-crustal magmatic sheets in the Cascades Mountains, Washington: implications for magma ascent. *Journal of Structural Geology, 20*(9-10), 1345-1363. doi:10.1016/s0191-8141(98)00072-8

Pyle, D. M., & Elliott, J. R. (2006). Quantitative morphology, recent evolution, and future activity of the Kameni Islands volcano, Santorini, Greece. *Geosphere, 2*(5), 253-268. doi:10.1130/ges00028.1

Rubin, A. M. (1995). Getting granite dikes out of the source region. *Journal of Geophysical Research-Solid Earth, 100*(B4), 5911-5929. doi:10.1029/94jb02942

Segall, P. (2016). Repressurization following eruption from amagma chamber with a viscoelastic aureole. *Journal of Geophysical Research-Solid Earth, 121*(12), 8501-8522. doi:10.1002/2016jb013597

Sigurdsson, H., Carey, S., Alexandri, M., Vougioukalakis, G., Croff, K., Roman, C., . . . Nomikou, P. (2011). Marine investigations of Greece's Santorini Volcanic Field. *Eos (Transactions, American Geophysical Union), 87*(34), 337-342.

Singer, B., Anderson, N., Le Mevel, H., Feigl, K., DeMets, C., Tikoff, B., . . . Vazquez, J. (2014). Dynamics of a large, restless, rhyolitic magma system at Laguna del Maule, southern Andes, Chile. *GSA today, 24*(12). doi:10.1130/GSATG216A.1

Singer, B., Le Mevel, H., Licciardi, J., Cordova, L., Tikoff, B., Garibaldi, N., . . . Feigle, K. (2018). Geomorphic expression of rapid Holocene silicic magma reservoir growth beneath Laguna del Maule, Chile. *Science Advances, 4*(6). doi:10.1126/sciadv.aat151

Smith, V. C., Isaia, R., & Pearce, N. J. G. (2011). Tephrostratigraphy and glass compositions of post-15 kyr Campi Flegrei eruptions: implications for eruption history and chronostratigraphic markers. *Quaternary Science Reviews, 30*(25-26), 3638-3660. doi:10.1016/j.quascirev.2011.07.012

Snyder, D., & Tait, S. (1995). Replenishment of magma chambers: Comparison of fluid-mechanic experiments with field relations. *Contributions to Mineralogy and Petrology, 122*(3), 230-240. doi:10.1007/s004100050123

Sparks, R. S. J., Francis, P. W., Hamer, R. D., Pankhurst, R. J., Ocallaghan, L. O., Thorpe, R. S., & Page, R. (1985). Ignimbrites of the Cerro Galan caldera, NW Argentina. *Journal of Volcanology and Geothermal Research, 24*(3-4), 205-248. doi:10.1016/0377-0273(85)90071-x

960 Stock, M., Humphreys, M., Smith, V., Isaia, R., Brooker, R., & Pyle, D. (2018). Tracking
961 Volatile Behaviour in Sub-volcanic Plumbing Systems Using Apatite and Glass:
962 Insights into Pre-eruptive Processes at Campi Flegrei, Italy. *Journal of Petrology, 0*, 1-29.
963 doi:10.1093/petrology/egy020
964 Stock, M. J., Humphreys, M. C. S., Smith, V. C., Isaia, R., & Pyle, D. M. (2016). Late-stage
965 volatile saturation as a potential trigger for explosive volcanic eruptions. *Nature*
966 *Geoscience, 9*(3), 249-U290. doi:10.1038/ngeo2639
967 Sudo, Y., & Kong, L. S. L. (2001). Three-dimensional seismic velocity structure beneath Aso
968 Volcano, Kyushu, Japan. *Bulletin of Volcanology, 63*(5), 326-344.
969 doi:10.1007/s004450100145
970 Tait, S., Jaupart, C., & Vergniolle, S. (1989). Pressure, gas content and eruption periodicity of a
971 shallow, crystallizing magma chamber. *Earth and Planetary Science Letters, 92*(1), 107-
972 123. doi:10.1016/0012-821x(89)90025-3
973 White, S. M., Crisp, J. A., & Spera, F. J. (2006). Long-term volumetric eruption rates and
974 magma budgets. *Geochemistry Geophysics Geosystems, 7*. doi:10.1029/2005gc001002
975 Wiebe, R. A. (1994). Silicic magma chambers as traps for basaltic magmas -- the Cadillac
976 Mountain intrusive complex, Mount Desert Island, Maine. *Journal of Geology, 102*(4),
977 423-437. doi:10.1086/629684
978 Wiebe, R. A., & Collins, W. J. (1998). Depositional features and stratigraphic sections in granitic
979 plutons: implications for the emplacement and crystallization of granitic magma. *Journal*
980 *of Structural Geology, 20*(9-10), 1273-1289. doi:10.1016/s0191-8141(98)00059-5
981 Wilson, C. J. N., Houghton, B. F., McWilliams, M. O., Lanphere, M. A., Weaver, S. D., &
982 Briggs, R. M. (1995). Volcanic and structural evolution of Taupo Volcanic Zone, New
983 Zealand -- a review. *Journal of Volcanology and Geothermal Research, 68*(1-3), 1-28.
984 doi:10.1016/0377-0273(95)00006-g
985 Woods, A. W., & Huppert, H. E. (2003). On magma chamber evolution during slow effusive
986 eruptions. *Journal of Geophysical Research-Solid Earth, 108*(B8).
987 doi:10.1029/2002jb002019
988 Zhang, Y. X. (1999). Exsolution enthalpy of water from silicate liquids. *Journal of Volcanology*
989 *and Geothermal Research, 88*(3), 201-207. doi:10.1016/s0377-0273(98)00115-2
990 Zollo, A., Maercklin, N., Vassallo, M., Dello Iacono, D., Virieux, J., & Gasparini, P. (2008).
991 Seismic reflections reveal a massive melt layer feeding Campi Flegrei caldera.
992 *Geophysical Research Letters, 35*(12). doi:10.1029/2008gl034242

993

994